Available online at www.sciencedirect.com

Journal of the European Ceramic Society 25 (2005) 509–520

www.elsevier.com/locate/jeurceramsoc

Phase evolution and crystallization in Si–B–C–N ceramics derived from a polyborosilazane precursor: microstructural characterization

Narayanan Janakiraman[a,*], Achim Zern[a,1], Markus Weinmann[a],
Fritz Aldinger[a], Paramanand Singh[b]

[a] *Pulvermetallurgisches Laboratorium, Max-Planck Institut für Metallforschung and Institut für Nichtmetallische Anorganische Materialien, Heisenbergstr. 3, D-70569 Stuttgart, Germany*
[b] *Department of Metallurgical Engineering, Indian Institute of Technology Madras, Chennai 600036, India*

Received 3 March 2002; received in revised form 3 March 2004; accepted 13 March 2004
Available online 21 July 2004

Abstract

Amorphous Si–B–C–N ceramic powder samples obtained by thermolysis of polyborosilazane $\{B[C_2H_4Si(H)NH]_3\}_n$ were isothermally annealed at different temperatures (1400–1800 °C) and hold-times (3, 10, 30, 100 h). Scanning electron microscopy (SEM) of annealed powders as well as polished cross sections of large powder particles from selected samples were carried out to study surface morphology, crystallization and associated microstructural changes. Microstructural and phase evolution were additionally investigated using high-resolution transmission electron microscopy (HRTEM) and energy filtering TEM (EFTEM). Higher surface areas of the powders were found to promote vapor-phase decomposition reactions resulting in SiC whisker growth. In coarser powders the influence of surface is manifested as a skin-core effect, where the 'skin' has undergone a higher degree of decomposition accompanied by an increased SiC crystal growth, compared to the 'core.' Crystallization of SiC occurs already at 1400 °C, although Si_3N_4 crystallization occurs only at 1700 °C, after more than 3 h of annealing.

Keywords: Precursors-organic; Nanocomposites; Whiskers; Electron microscopy; Si–B–C–N

1. Introduction

Quaternary Si–B–C–N ceramics synthesized by thermolysis of suitable organometallic precursors frequently possess an enhanced thermo-chemical stability at temperatures exceeding 2000 °C.[1–11] It is supposed that due to the formation of a turbostratic B–C–N phase[12–14] thermodynamically expected decomposition reactions[15] are kinetically retarded. Recent publications by Müller et al.[7,16] have reported in detail on the influence of the chemical composition of this phase, i.e., the Si:B:N ratio, on the crystallization and decomposition of Si–B–C–N ceramics derived from different boron-modified polysilazanes.

In a previous paper, we reported the overall phase evolution and crystallization in amorphous Si–B–C–N ceramic powder samples obtained from thermolysis of polyborosilazane $\{B[C_2H_4Si(H)NH]_3\}_n$, subjected to high-temperature annealing.[17] Apart from the annealing temperature and isothermal hold-time, the strong influence of the surface area of the powders on the crystallization and decomposition reactions was reported. Here, we present the microstructural characterization of the same materials, in an attempt to understand the local compositional and structural changes associated with the above reactions.

2. Experimental procedure

2.1. Materials

Thermolysis of $\{B[C_2H_4Si(H)NH]_3\}_n$ (referred to as MW33) in alumina Schlenk tubes in a flowing Ar atmosphere at a heating rate of 1 °C/min to the final temperature of 1400 °C yielded an amorphous ceramic residue.[6] This was further crushed and sieved into four powder size fractions: >315, 80–315, 32–80, and <32 μm; code named as MW33VC, MW33IC, MW33C, and MW33F, respectively.

---

[*] Corresponding author.
E-mail address: badhri@mf.mpg.de (N. Janakiraman).
[1] Present address: Balluff GmbH, Gartenstr. 21-25, D-73765 Neuhausen a.d.F., Germany.

0955-2219/$ – see front matter © 2004 Elsevier Ltd. All rights reserved.
doi:10.1016/j.jeurceramsoc.2004.03.010

The powders were isothermally annealed at various temperatures from 1400–1800 °C in steps of 100 °C in a nitrogen atmosphere (1030 mbar) using carbon crucibles in a graphite furnace (heating rate: 10 °C/min up to 1400 °C, thereafter at 2 °C/min up to the final hold temperature). Hold-times were 3, 10, and 30 h.

2.2. *Scanning electron microscopy (SEM)*

SEM investigations were carried out on as annealed powders as well as on polished cross sections of large powder particles from selected samples. As annealed powders were examined using a digital scanning microscope model ZEISS DSM 982 Gemini. EDX analyses were performed using an EDX system model Link-ISIS 300, Oxford Instruments with an ultra-thin window and a high-resolution Germanium detector. Powders were dispersed on double side adhesive carbon tapes. A JEOL JSM 6300F was employed for observing polished cross sections of large powder particles. Samples were prepared using standard metallographic techniques.

2.3. *Transmission electron microscopy (TEM)*

Samples annealed at lower temperatures were studied by high-resolution (HR) TEM using an analytical electron microscope (AEM) model JEOL JSM 4000 EX. Electron spectroscopic imaging (ESI) using an energy filtering technique (EFTEM) was used to characterize the phase evolution, elemental distribution and overall microstructure of samples annealed at higher temperatures using an energy filtering TEM model ZEISS 912 Ω. Elemental distribution maps for silicon, carbon, nitrogen, and boron were obtained using the "three window technique."[18] TEM samples were prepared by fixing annealed powder particles (∼1–2 mm) inside a copper ring by gluing, followed by grinding, dimpling and ion milling. Fragile particles were glued into a slit contained in 3 mm diameter alumina cross-section holders, from which thin discs were obtained by mechanical sectioning. These discs were then further prepared using the standard procedure.

3. Results and discussion

3.1. *Scanning electron microscopy investigations of annealed powders*

3.1.1. *General observations on whisker growth*

Optical microscopy and SEM observations showed contrasting features between VC, IC, C and F powders annealed at different temperatures. VC powders, which have the highest particle size among the investigated samples, showed no surface features at any temperature. An SEM image of MW33VC annealed at 1800 °C/10 h is shown in Fig. 1. In other powders, annealing at 1600 °C and above resulted in a change in the color of the annealed powder mass from black to dull gray/dull green. At 1700 °C, the top layer of the IC and C powder changed to light green/light yellow. Under optical microscope, a dense network of whiskers was observed in these regions. At still higher temperatures the color changed back to dull gray and black, signifying a reduction in the amount of whiskers. The extent of whisker growth and the temperature for maximum growth varied with the particle size of the annealed powders. Very coarse powders showed no whisker growth at any temperature. In intermediate coarse (IC) powders nucleation of whiskers started at 1600 °C. Growth was highest at 1700 °C and decreased at 1800 °C. In coarse (C) powders whisker growth started as early as 1600 °C for 3 h annealing and was highest in the temperature range of 1600–1700 °C. At longer annealing times at 1700 and 1800 °C, growth decreased. In our earlier report,[17] we have shown by thermogravimetry (TG) and XRD analyses that the onset of decomposition and crystallization processes begin at lower annealing temperatures and proceed rapidly to completion, in powders of progressively decreasing particle size (increasing surface area). Observation of a higher amount of whisker growth in finer powders indicates that in this regard decomposition of silicon nitride plays an important role. Intermediate coarse (IC) powder samples, which have a particle size between those of VC and C powders were chosen for detailed investigations. SEM images of MW33IC powders annealed at 1700 and 1800 °C/10 h are given in Figs. 2(a–d) and 3(a–d), respectively. While the whiskers have nucleated and grown on the surface of large powder particles, the surface of the particles themselves is smooth and devoid of any surface crystallization. Comparing Figs. 2(a) and 3(a), it is clear that the amount of whiskers is less in the 1800 °C sample than in the 1700 °C sample. EDX analyses of whiskers at different locations clearly show peaks at 1.75 and 0.25 keV corresponding to silicon and carbon, respectively, indicating that the whiskers are silicon carbide (Figs. 2(e) and 3(e)).

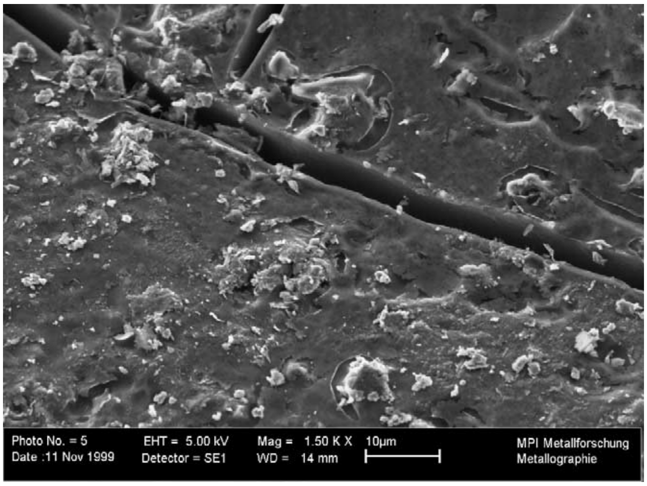

Fig. 1. SEM image of MW33VC sample annealed at 1800 °C/10 h/1030 mbar N_2. Surface of as annealed powder is devoid of whisker growth.

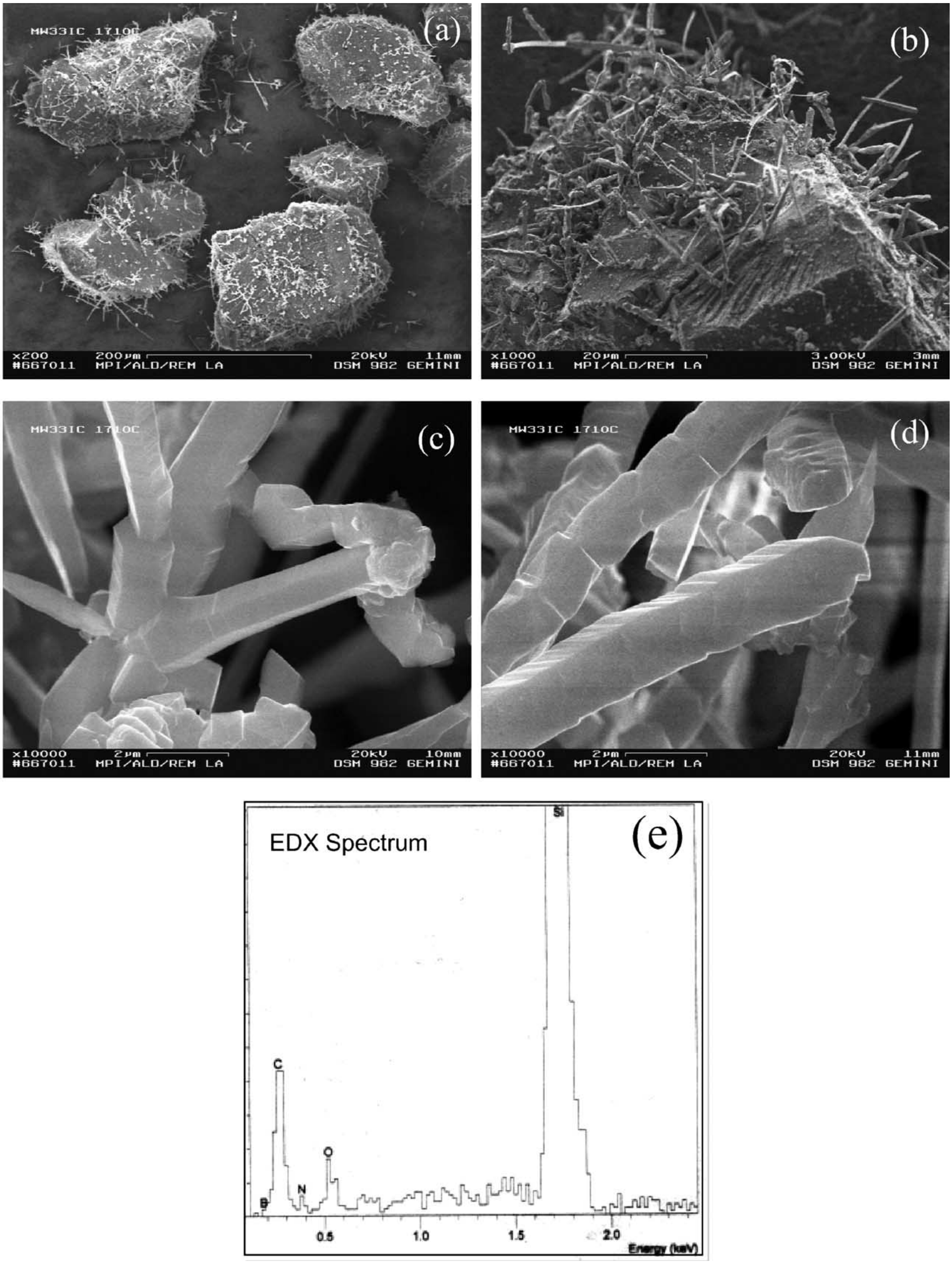

Fig. 2. SEM images of whisker growth on the surface of MW33IC powder sample annealed at 1700 °C/10 h/1030 mbar N_2. EDX analysis confirms that whiskers are SiC.

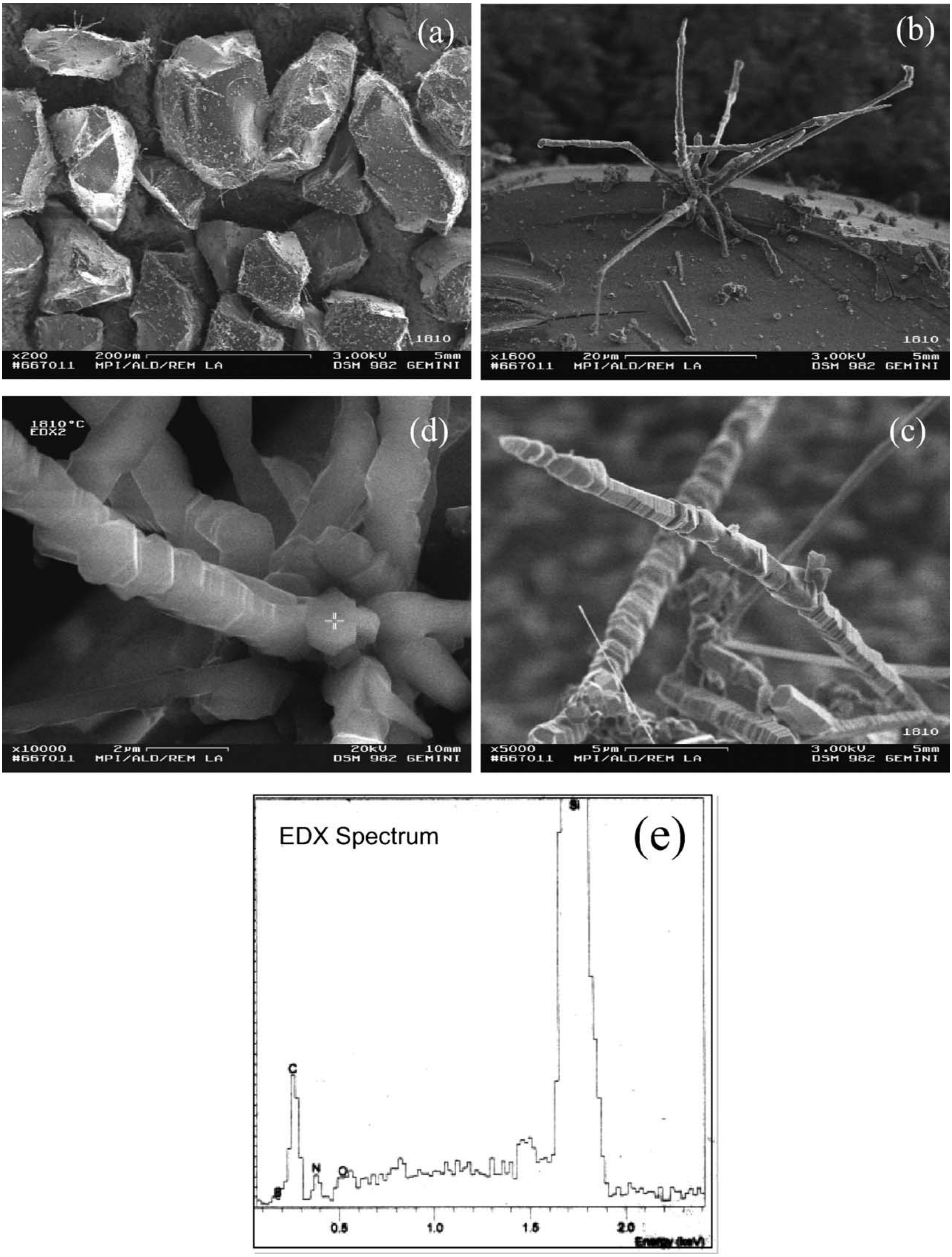

Fig. 3. SEM images of whisker growth on the surface of MW33IC powder sample annealed at 1800 °C/10 h/1030 mbar N_2. Note that the amount of whiskers is less as compared to the 1700 °C/10 h/1030 mbar N_2 annealed powders.

3.1.2. Whisker morphology

SEM images at higher magnifications reveal the morphology of the whiskers. Whiskers from the 1700 °C sample have a hexagonal cross section although a considerable amount of whiskers show rectangular and rounded cross-sections. Also, the majority of whiskers show axial discontinuities and stepped growth. Some whiskers have a knotted structure with side branching. Whiskers in the 1800 °C sample

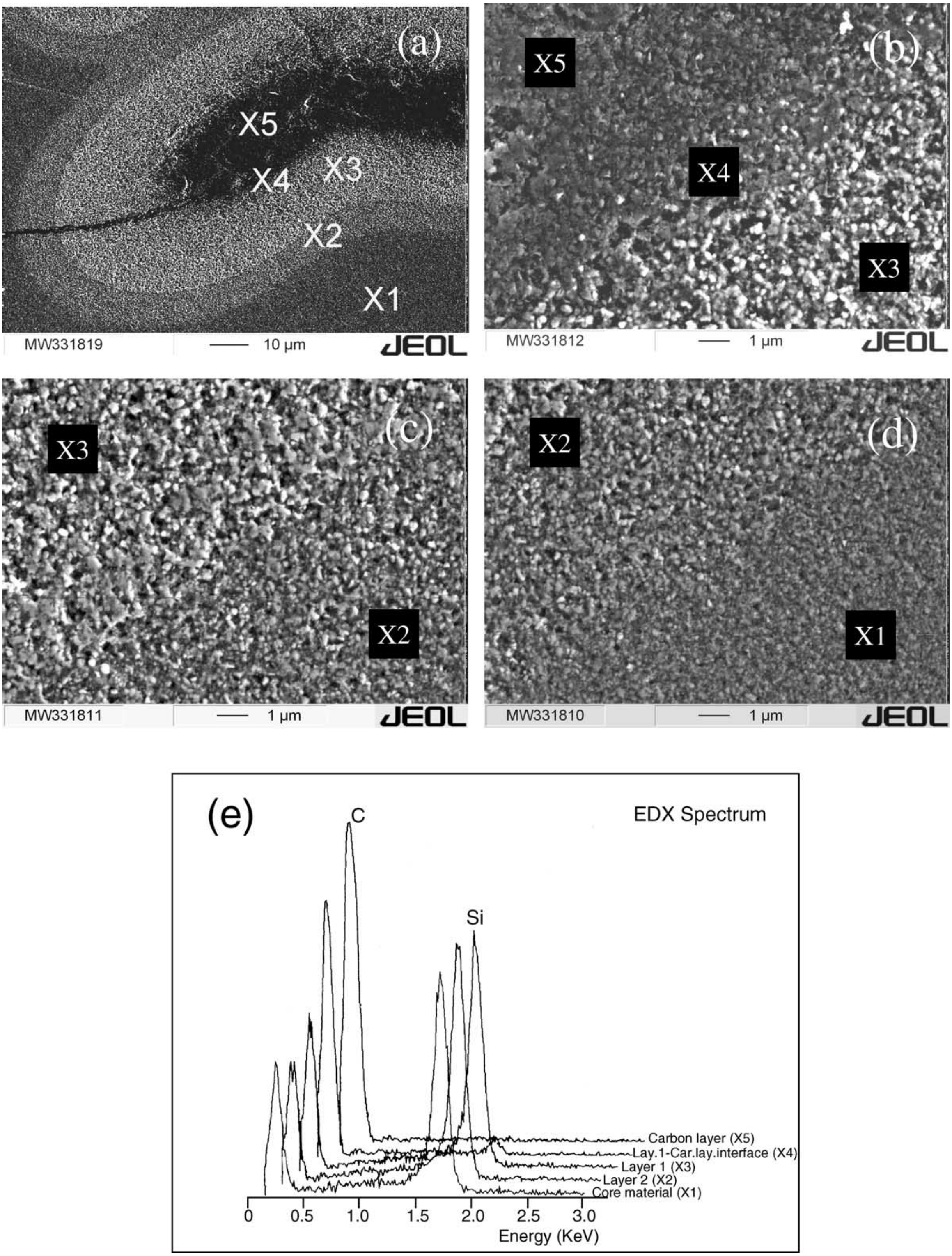

Fig. 4. SEM micrographs from MW33VC sample annealed at 1800 °C/10 h/1030 mbar N_2—polished cross-section showing the layered microstructure. A comparison of EDX analysis indicates the progressive increase in carbon content from core to surface.

are mostly of hexagonal cross section, with hexagonal platelets stacked in the growth direction. In some whiskers regularly stacked platelets are interrupted by regions of rounded/irregular cross section where side branching occurs.

3.1.3. Growth mechanism and structure

Generally SiC whiskers are known to grow from a gas phase. Present observations (Section 3.1.1) indicate that SiC whisker growth occurs concomitant with the decomposition reactions. Although the carbothermal reduction reaction $Si_3N_4 + 3C = 3SiC + 2N_2$ can result in the formation of silicon carbide (which in fact does occur as will be discussed in Section 3.2), growth in the form of whiskers requires mass transportation through a liquid or a gas phase. SEM images of the whiskers could not detect any liquid phase at the tip of whiskers catalyzing the growth by vapor–liquid–solid (VLS) mechanism. However, qualitative EDX investigations of whiskers from the 1700 °C/10 h sample pointed to a small quantity of oxygen, apart from silicon and carbon (Fig. 2(e)). Considering the fact that powders of higher surface area show maximum whisker growth, the role of adsorbed oxygen on the surface of the powders becomes important. Such low quantities of oxygen in an otherwise inert atmosphere as in the present case, leads to active oxidation of Si–B–C–N material (either in amorphous or crystalline state). The resultant silicon monoxide and carbon monoxide then feed the homogeneous (gas–gas) or heterogeneous (gas–solid) reactions.[19]

$$SiO_{(g)} + CO_{(g)} = SiC_{(s)} + O_{2(g)} \quad (1)$$

$$SiO_{(g)} + 2C_{(s)} = SiC_{(s)} + CO_{(g)} \quad (2)$$

Growth is initiated at a screw dislocation, where atoms are added at the dislocation step, and is promoted along the dislocation axis, which is generally [0 0 0 1] for α-SiC whiskers and [1 1 1] for β-SiC whiskers. For whiskers with hexagonal cross-section, it is presumed that these are of α-type although β-SiC whiskers, having different cross-sections, are present. Indeed, XRD investigations indicate crystallization of α-SiC at and above 1700 °C.[17]

3.2. SEM investigations of polished cross sections of annealed MW33VC powders

3.2.1. General comments

The preceding discussion and also our earlier studies[17] indicate that surfaces provide active reaction sites for decomposition and crystallization reactions. Although this is not obvious from the SEM images of as annealed VC powder surfaces, it is expected that the increased extent of such reactions at surface and near-surface regions rather than in the powder core, should be reflected in the microstructure of the respective regions. To verify this, cross sections of annealed powders MW33VC powders of size ranging from 1 to 2 mm were examined under SEM.

3.2.2. Skin-core effect

Cross section of the 1800 °C/10 h sample shows a layered structure at the surfaces and cracks covering the entire particle. SEM micrograph of the layered structure at a crack tip is given in Fig. 4(a). The outermost dark layer is followed by two porous layers and finally the core structure. Micrographs of the interfaces between the single layers and finally with the core are given in Fig. 4(b–d), respectively. They show a progressively increased degradation of the material from the core to the surface. Similar layered structure suggesting enhanced degradation at the surface regions were also observed in samples annealed at 1700 °C/10 h, although with lower layer thickness and resolution. A comparison of EDX analysis of the layers (Fig. 4(e)) suggests a progressive increase in carbon towards the surface. The dark layer (X1) finally shows only the carbon peak. Such a skin-core effect has been previously reported for Si–C–O and Si–C–N–O fibers,[20–22] where carbon enrichment accompanied by depletion of silicon, nitrogen and oxygen has been observed.

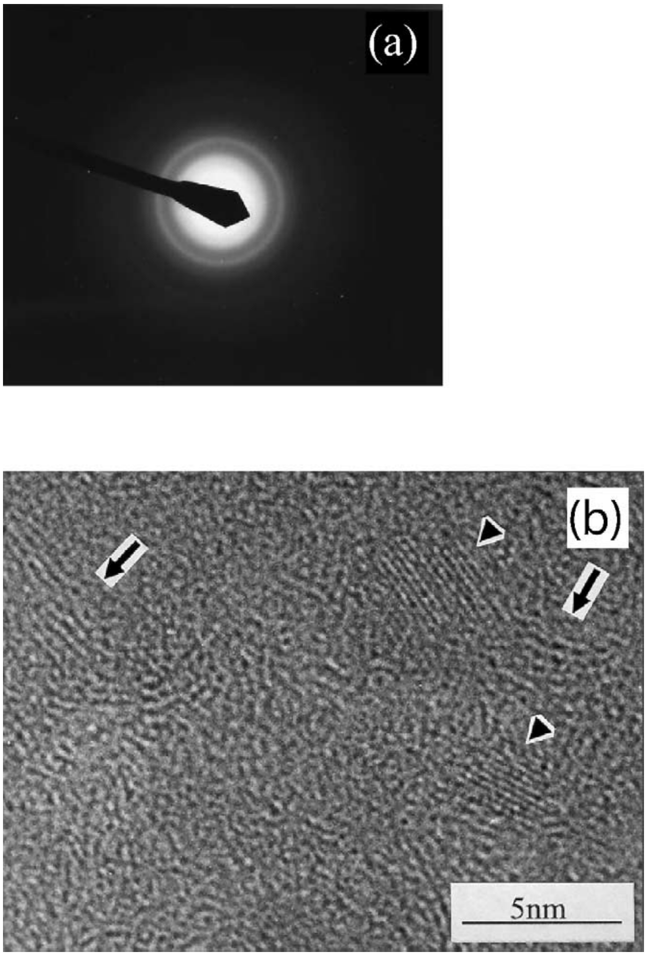

Fig. 5. SAD pattern (a) and high-resolution TEM image (b) of MW33VC sample annealed at 1400 °C/10 h/1030 mbar N_2.[14]

In such oxygen-cured systems, thermal degradation of the material involves removal of silicon and carbon in the form of SiO and CO, respectively. As the ceramics investigated here are oxygen-free, decomposition reactions involving SiO and CO should have taken place only with the aid of adsorbed oxygen on powder surfaces, as discussed above (compare discussion on whisker growth). While extent of decomposition arising from the active oxidation is limited by the amount of adsorbed oxygen, the carbothermal reduction reaction ($Si_3N_{4(s)} + 3C_{(s)} = 3SiC_{(s)} + 2N_{2(g)}$) due to the presence of "free" carbon is still favoured at the surface and near surface regions,[15] where the gaseous by-product nitrogen can be easily removed to carry the reaction forward. The decomposition-assisted crystallization is evidenced from the formation of large SiC grains observed in the layer lying just below the carbon layer, resulting from the above reaction. The number and size of SiC grains decrease proceeding towards the powder core. In the core of the powder, this reaction is kinetically hindered, due to the longer diffusion distance for nitrogen. Longer diffusion pathways are directly connected with an increasing nitrogen partial pressure, which shifts the onset of Si_3N_4 decomposition to higher temperatures.[15] These observations are further confirmed by TEM investigations as will be discussed in Section 3.3.2.

3.3. *Transmission electron microscopy*

3.3.1. *Conventional and high-resolution TEM*

Two samples of MW33VC annealed for 10 h at 1400 °C[14] and 1500 °C were studied under conventional and high-resolution TEM. The results are presented in Figs. 5 and 6, respectively. In the bright field images (BF), here only the 1500 °C sample is shown in Fig. 6(b), crystallites of SiC appearing as dark spots in a predominantly amorphous matrix with sizes ranging from 2 to 10 nm could be observed. The population of finer crystallites was higher in 1400 °C/10 h sample (not shown). The corresponding diffraction ring patterns are given in Figs. 5(a) and 6(a), respectively. The inner most diffused ring corresponds to the B–C–N layers having a turbostratic structure. The next bright ring is comprised of reflections from $(1\,1\,1)_{\beta\text{-SiC}}$, $(1\,0\,2)_{\alpha\text{-SiC}}$, and $(1\,0\,3)_{\alpha\text{-SiC}}$. Bright spots appear along this ring at a $1/d$ value corresponding to the $(1\,1\,1)_{\beta\text{-SiC}}$ reflection ($3.97\,nm^{-1}$; $d = 2.516$ Å), indicating the presence of β-SiC crystallites. This is further confirmed by the observation of two characteristic rings at 6.49 and $7.61\,nm^{-1}$ ($d = 1.540$ and 1.314 Å, respectively) corresponding to the $(2\,2\,0)_{\beta\text{-SiC}}$ and $(3\,1\,1)_{\beta\text{-SiC}}$ reflections. Also a faint ring at $4.59\,nm^{-1}$ is observed which corresponds to the $(2\,0\,0)_{\beta\text{-SiC}}$ reflection. Presence of β-Si_3N_4 crystallites in the sample

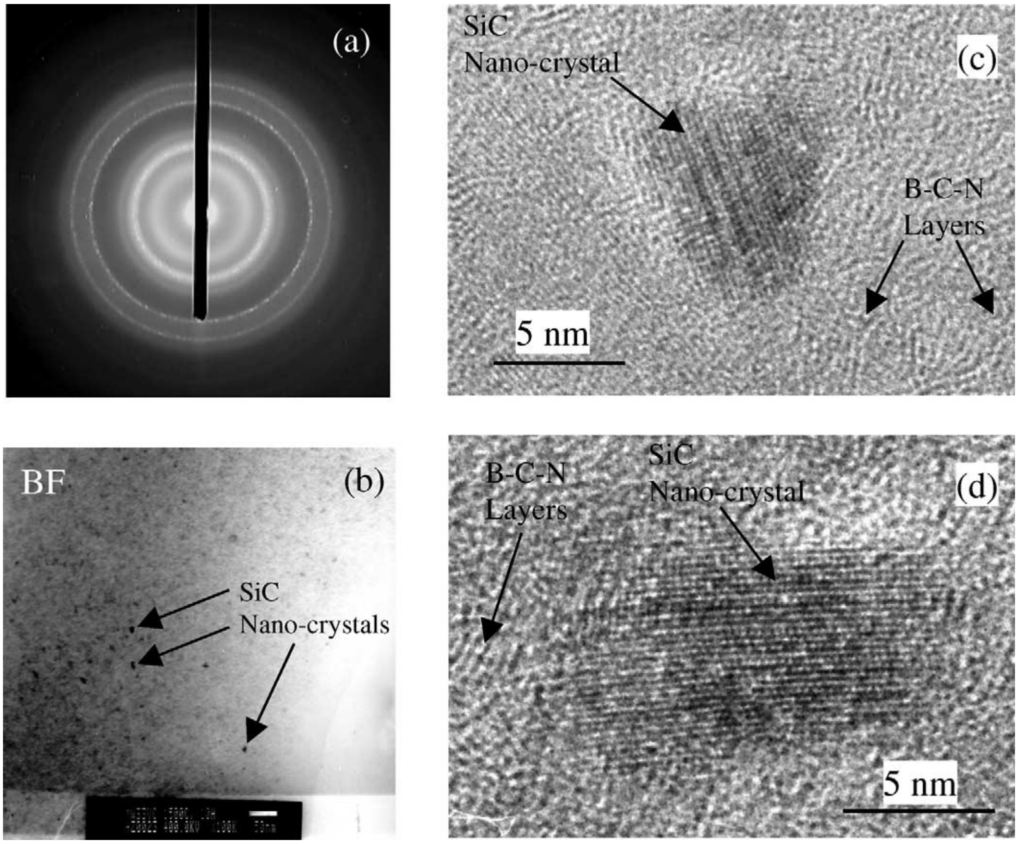

Fig. 6. SAD pattern (a), conventional bright field, (b) and high-resolution TEM images (c and d) of MW33VC sample annealed at 1500 °C/10 h/1030 mbar N_2.

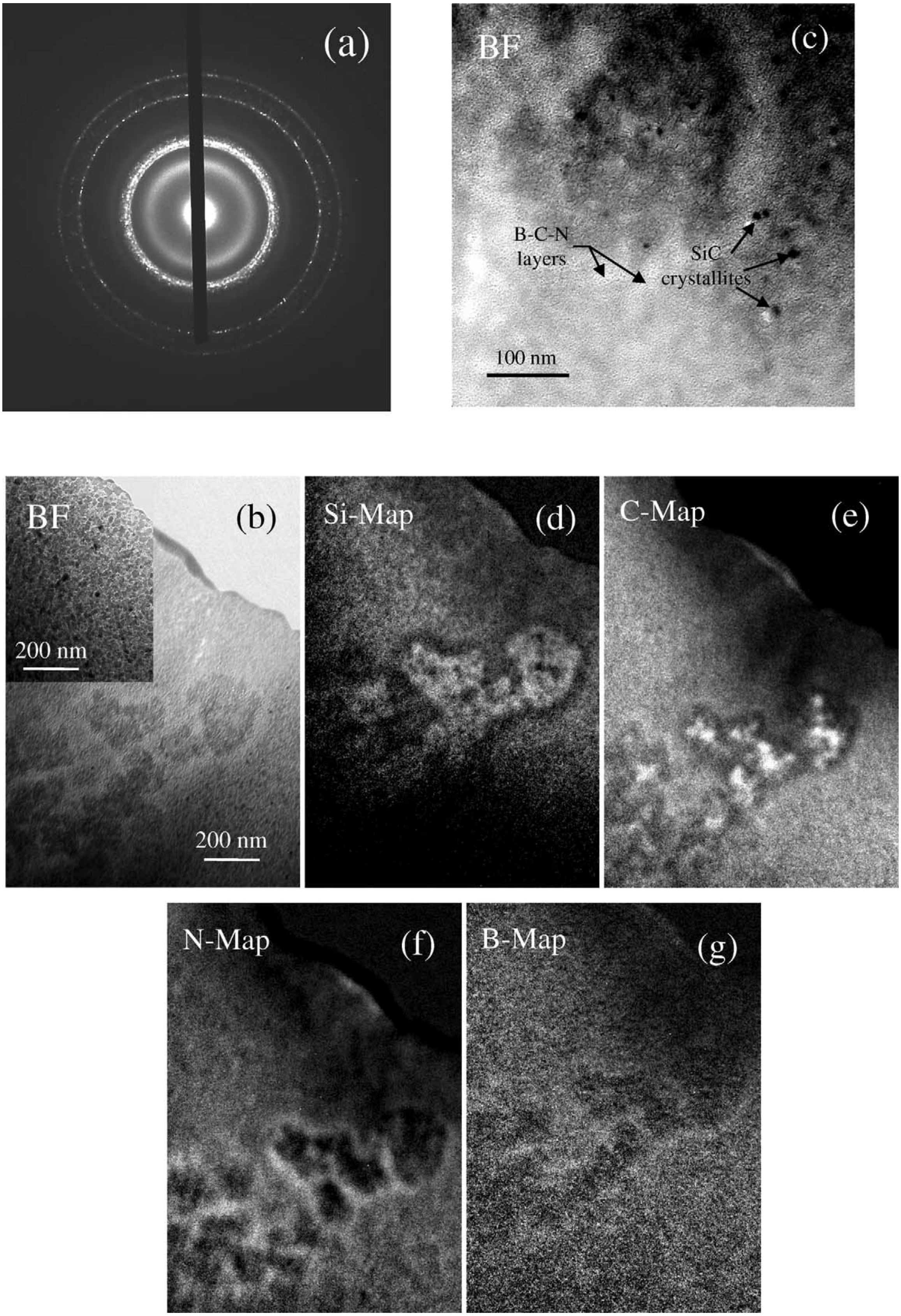

Fig. 7. Conventional and energy filtering TEM analysis of MW33VC powder sample annealed at 1700 °C/3 h/1030 mbar N_2. BF images in (b) show the difference in the extent of crystallization between core and surface regions (inset). Elemental maps (d–g) show the associated chemical segregation in regions near the surface.

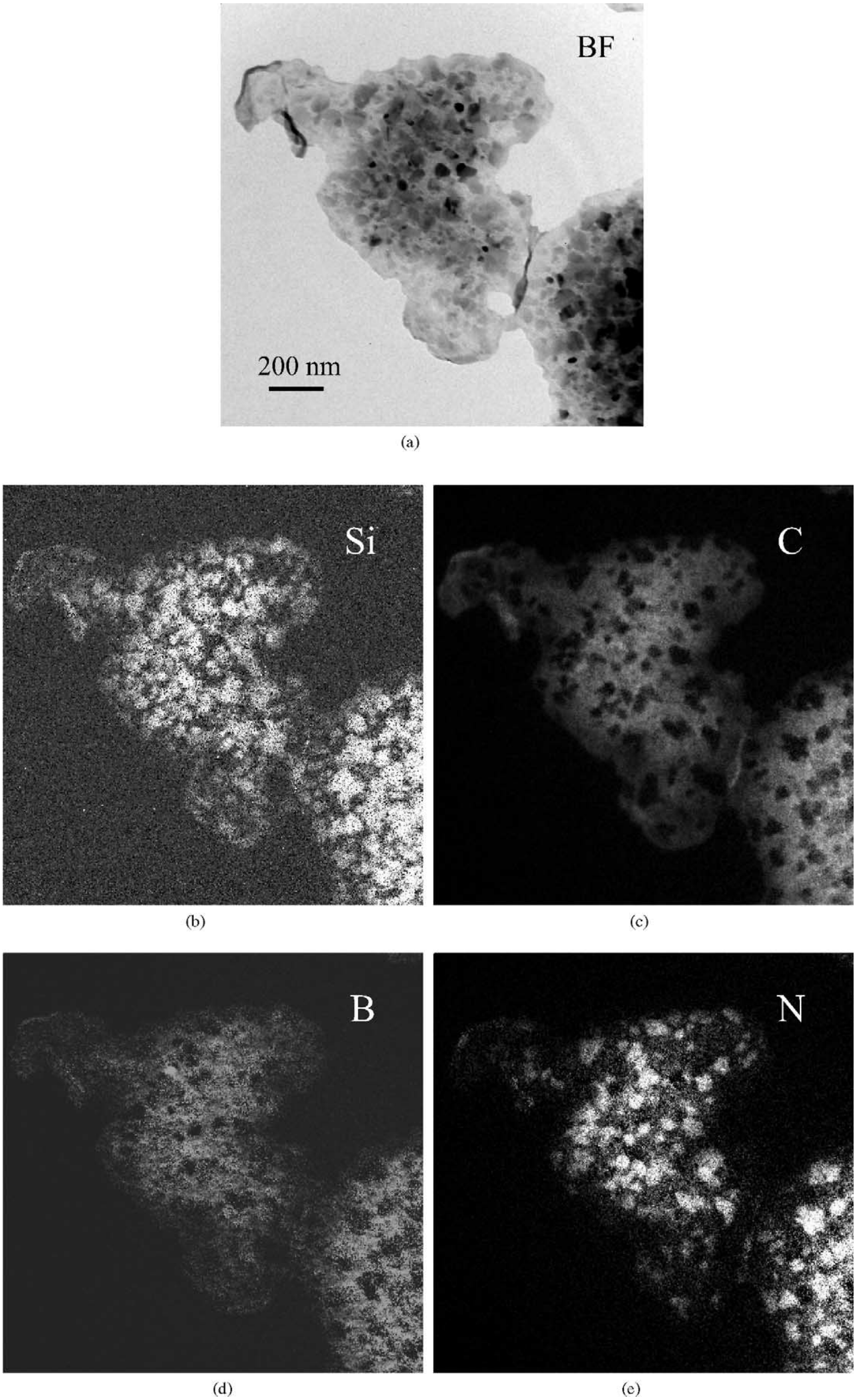

(a)

(b) (c)

(d) (e)

Fig. 8. Bright field image and elemental maps of the core region of MW33VC powder sample annealed at 1800 °C/10 h/1030 mbar N_2. SiC and Si_3N_4 crystals are equally distributed in a B–C–N matrix phase.

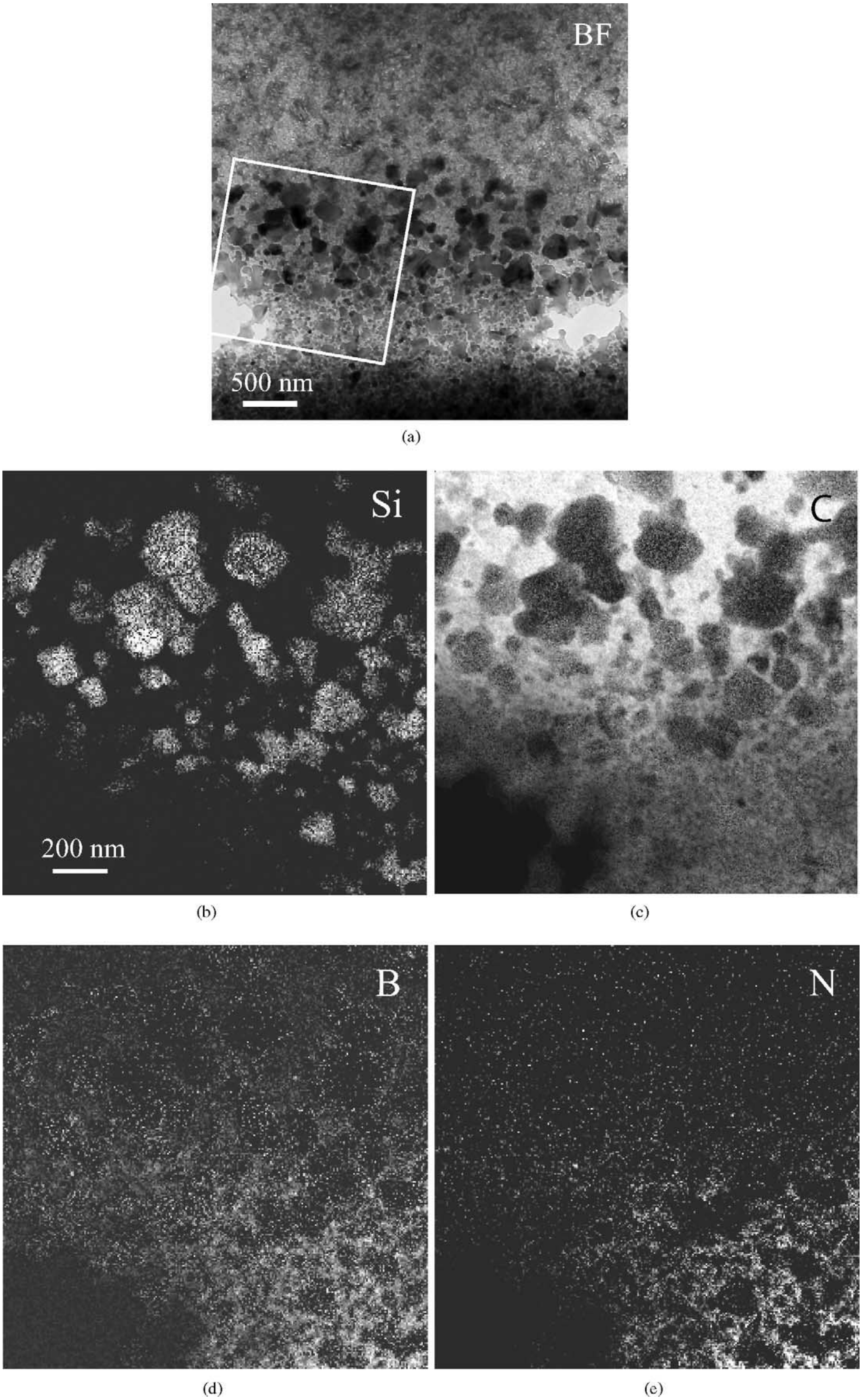

(a)

(b)

(c)

(d)

(e)

Fig. 9. Bright field image and elemental maps of the near surface region of MW33VC powder sample annealed at 1800 °C/10 h/1030 mbar N_2. BF image obtained at lower magnification (4000×) shows the layered microstructure. Elemental maps obtained at a higher magnification (10 000×) from the area enclosed in the box in BF image show the chemical concentration gradients from surface to the core.

can be excluded due to the absence of (dotted) diffraction rings at 3.03 nm^{-1} (3.293 Å) and 2.63 nm^{-1} (3.80 Å) corresponding to the $(2\,0\,0)_{\beta\text{-}Si_3N_4}$ and $(1\,1\,0)_{\beta\text{-}Si_3N_4}$ reflections. Fig. 6(c and d) are the high-resolution images of two SiC crystallites obtained at a magnification of 400K×. Measurement of the '*d*' spacing between them indicates that they are $(1\,1\,1)_{\beta\text{-}SiC}$ planes with an interplanar distance of 2.516 Å. The images also show the turbostratic B–C–N layers[12,13] with an interplanar spacing of ∼3.64 Å. No preferred orientation of SiC planes with respect to the B–C–N layers could be observed from the images.

3.3.2. Energy filtering TEM

XRD investigations[17] show that silicon nitride does not crystallize below annealing temperatures of 1700 °C. At 1700 °C/10 h annealing, peaks of Si_3N_4 were observed unequivocally. XRD pattern of sample annealed at 1700 °C/3 h shows only a small shoulder on the left of $(1\,1\,1)_{\beta\text{-}SiC}$, possibly from the $(1\,0\,1)_{\beta\text{-}Si_3N_4}$ planes, while corresponding reflections from $(2\,0\,0)_{\beta\text{-}Si_3N_4}$ or $(1\,1\,0)_{\beta\text{-}Si_3N_4}$ planes were missing. Thus, the 1700 °C/3 h sample was chosen to examine the onset of Si_3N_4 phase separation. However, no crystalline Si_3N_4 could be detected from the SAD pattern (Fig. 7(a)). Fig. 7(b) shows the BF image of the sample obtained from the powder core while the inset shows the BF image from near the powder surface. Microstructures of the two regions are strikingly different, with the region near the surface containing relatively coarse grains in large numbers while the core region is predominantly amorphous with relatively finer grains in smaller numbers. This observation is in accordance with the previous results from SEM investigations.

Additionally, the BF image of the core region shows a dark heterogeneity extending across the middle of the image. A portion of the same in higher magnification (31 500×) is given in Fig. 7(c). In order to further investigate this heterogeneity, electron spectroscopic imaging was employed. Accordingly, elemental maps of silicon, carbon, nitrogen and boron were obtained and are given in Fig. 7(d–g). In the silicon map, the heterogeneity appears as a brighter area indicating that it is rich in silicon compared to the surrounding matrix. However, central regions in the silicon map of the heterogeneity that appear dark are bright in the carbon map. This may indicate that carbon rich central regions are surrounded by regions rich in silicon and carbon, presumably in the form of SiC. From the silicon map it is further observed that a dark layer surrounds silicon rich (bright) regions. This layer appears bright, both in nitrogen and boron maps indicating boron nitride enrichment. In total, the variations in elemental concentration can be thought of as regions of phases C, SiC + C, SiC + BN, BN and finally the matrix containing SiC, amorphous Si–C–N and B–C–N phases, moving outwards from the center of the heterogeneity. This is probably a location, where a crack or surface pore partially extends into the bulk of the powder particle, near the region of examination.

In samples annealed at 1800 °C/10 h, again two regions were studied: one, the core region and the other, the surface region. BF image from the core region is given in Fig. 8(a) and corresponding elemental maps of Si, C, N and B are given in Fig. 8(b–e). The microstructure shows a homogeneous distribution of approximately equally sized nano-crystals of SiC and Si_3N_4, embedded in an amorphous matrix. From the images the size of the grains is estimated as around 80 nm both for SiC and Si_3N_4.

BF image from the near surface region is given in Fig. 9(a). The image shows large grains (appearing as dark areas) embedded in a gray matrix. Elemental maps of Si, C, N and B obtained from a region at the lower left of the BF image are given in Fig. 9(b–e). The top portion of the carbon map is completely bright and the corresponding areas in other three maps are dark. This indicates that the region contains almost pure carbon. From silicon and carbon maps the large grains are identified as SiC embedded in the carbon matrix. Moving further downwards, a rather sharp reduction in carbon content is observed around the middle of the carbon map. Nitrogen and boron maps show a more gradual increase in nitrogen and boron except for the dark pockets, which are evidently SiC grains. However, no silicon nitride grains could be observed in the observed region, although they are present further downwards moving towards the matrix region. Thus, a layered structure is observed starting with a layer of pure carbon followed by layers of carbon and large SiC grains, intermediate SiC grains embedded in amorphous B–C–N phase and finally the matrix material consisting of nano-crystals of SiC, Si_3N_4 and amorphous B–C–N phase. A schematic picture of this layered phase distribution is depicted in Fig. 10. The above result confirms the earlier SEM observations of the surface regions in MW33VC sample, annealed at 1800 °C/10 h. All the above findings clearly indicate the progressively increased depletion of nitrogen boron and silicon by decomposition and active oxidation reactions, respectively, at higher annealing temperatures, and also the increased extent of such reactions near the surface regions.

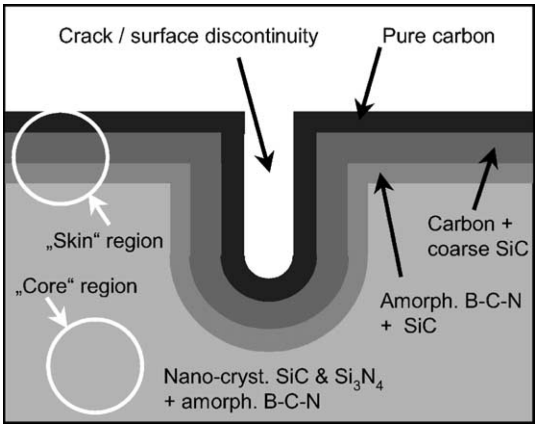

Fig. 10. Schematic picture of the phase distribution from surface to the core of the powder particles, forming a layered structure.

4. Conclusions

Phase evolution of an amorphous precursor-derived ceramic as a function of the particle size was investigated. Phase segregation occurred already at 1400 °C, with the formation of turbostratic B–C–N phase and crystallization of SiC nano-crystals. However, chemical modification of the inter-granular phase to initiate Si_3N_4 crystallization only takes place in coarse-grained ceramics at 1700 °C above 3 h of annealing. Specific surface area of the starting amorphous powders controls the crystallization and decomposition reactions. Because of their higher surface areas, finer powders most probably adsorb oxygen and/or water more easily than coarse-grained ceramics. Presence of oxygen aids in vapor phase decomposition reactions. In fine powders, this directly leads to SiC whisker growth, wherein the extent of whisker growth varies with the particle size. In coarser powders active oxidation and/or decomposition of the material occur, which is pronounced along the surface regions. This leads to a layered microstructure with a gradient in chemical composition from the surface to the core.

Acknowledgements

The authors wish to thank Mr. H. Labitzke and Ms. S. Kühnemann for their contribution in SEM analysis. Thanks to Dr. Y. Cai and Ms. S. Prinz for providing TEM results presented in Fig. 5. Deutscher Akademischer Austauschdienst (DAAD) and Deutsche Forschungsgemeinschaft (DFG) are acknowledged for the financial support.

References

1. Jansen, M., Baldus, H.-P., Ger. Offen. DE 410 71 08 A1 (1992).
2. Baldus, H.-P., Wagner, O. and Jansen, M., *Mater. Res. Soc. Symp. Proc.* 1992, **271**, 821.
3. Baldus, H.-P. and Jansen, M., *Angew. Chem.* 1997, **109**, 338; Baldus, H.-P., and Jansen, M., *Angew. Chem. Int. Ed. Engl.* 1997, **36**, 328.
4. Riedel, R., Kienzle, A., Dressler, W., Ruwisch, L., Bill, J. and Aldinger, F., *Nature* 1996, **382**, 796.
5. Riedel, R., Bill, J. and Kienzle, A., *Appl. Organomet. Chem.* 1996, **10**, 241.
6. Weinmann, M., Schuhmacher, J., Kummer, H., Prinz, S., Peng, J., Seifert, H. J. *et al.*, *Chem. Mater.* 2000, **12**, 623.
7. Müller, A., Gerstel, P., Weinmann, M., Bill, J. and Aldinger, F., *J. Eur. Ceram. Soc.* 2000, **20**, 2655.
8. Weinmann, M., In *Precursor-Derived Ceramics*, ed. J. Bill, F. Wakai and F. Aldinger. Wiley-VCH, Weinheim, 1999, p. 83.
9. Weinmann, M., Kamphowe, T. W., Schuhmacher, J., Müller, K. and Aldinger, F., *Chem. Mater.* 2000, **12**, 2112.
10. Weinmann, M., Nast, S., Berger, F., Müller, K. and Aldinger, F., *Appl. Organomet. Chem.* 2001, **15**, 867.
11. Weinmann, M., Zern, A., Hörz, M., Berger, F., Müller, K. and Aldinger, F., *Mat. Sci. Forum*. 2002, **286–388**, 335.
12. Jalowiecki, A., Bill, J., Aldinger, F. and Mayer, J., *Composites* 1996, **27A**, 717.
13. Jalowiecki, A., *TEM Investigations on the Demixing and Crystallization of Single-Phase Amorphous Precursor Ceramics.* Ph.D. thesis, Universität Stuttgart, Stuttgart, Germany, 1997 (in German).
14. Zimmermann, A., Bauer, A., Christ, M., Cai, Y. and Aldinger, F., *Acta Mater.* 2002, **50**(5), 1187.
15. Seifert, H. J., Lukas, H. L. and Aldinger, F., *Ber. Bunsenges. Phys. Chem.* 1998, **102**, 1309.
16. Müller, A., Gerstel, P., Weinmann, M., Bill, J. and Aldinger, F., *J. Eur. Ceram. Soc.* 2001, **21**, 2171.
17. Janakiraman, N., Weinmann, M., Schuhmacher, J., Müller, K., Bill, J., Aldinger, F. *et al.*, *J. Am. Ceram. Soc.* 2002, **85**(7), 1807–1814.
18. Mayer, J., Szabo, D. V., Rühle, M., Seher, M. and Riedel, R., *J. Eur. Ceram. Soc.* 1995, **15**, 717.
19. Monthioux, M. and Delverdier, O., *J. Eur. Ceram. Soc.* 1996, **16**, 721.
20. Delverdier, O., Monthioux, M., Mocaer, D. and Pailler, R., *J. Eur. Ceram. Soc.* 1993, **12**, 27.
21. Mocaer, D., Pailler, R., Naslain, R., Richard, C., Pillot, J., Dunogués, J. *et al.*, *J. Mater. Sci.* 1993, **28**, 2639.
22. Delverdier, O., Monthioux, M., Mocaer, D. and Pailler, R., *J. Eur. Ceram. Soc.* 1994, **14**, 313.